ELECTRONIC SUPPLEMENTARY MATERIAL

I. Supplementary Videos

Three supplementary videos are provided to help understand the experimental and numerical setup. Videos 1 and 2 (speeded up 4x) show experiments for LATEX ($W = 0.4$ m, $t = 100$ μm) and B0PP1 ($W = 0.2$ m, $t = 50$ μm), respectively. Video 1 shows a different perspective view of the experiment included in Fig. 1a of the main text. The frontal view in Video 2 shows the initial large fold observed for small indentation and the subsequent wrinkling of the film. The penetration length, ℓ, shown in the video marks the distance along which the indenter deforms the film. While the films are held horizontally in the experiments for LATEX, a different setup was used for thinner films to have them vertically oriented. Video 3 shows a numerical simulation in Abaqus for $W = 0.2$ m and $t = 0.5$ μm.

II. Numerical Method

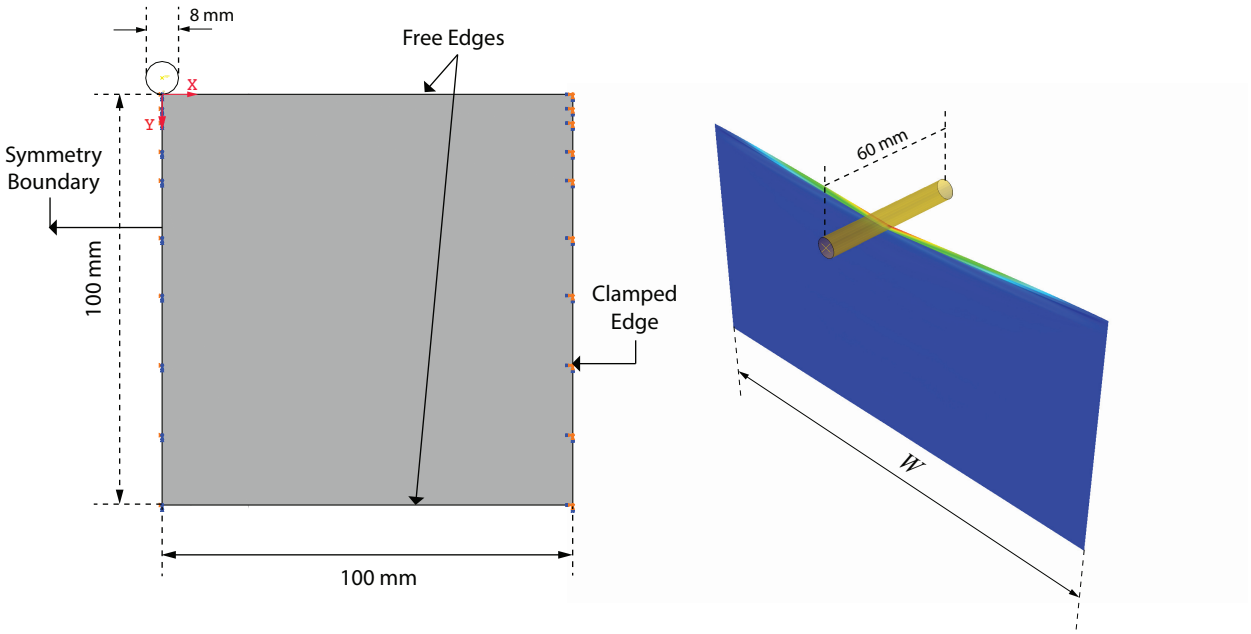

Fig. S 1. Schematic of the setup geometry used in the numerical simulations leading to Fig. 2 of the main text. The effective width of the system is $W = 200$ mm observed in the figure on the right after mirroring the simulation.

The numerical analysis was made in a 100×100 mm film meshed with S4R shell elements that was indented by a discrete rigid cylinder of radius $R = 4$ mm and length $D = 60$ mm. The film was completely clamped on one side and symmetric boundary conditions (XSYMM option) were applied to the opposite side (see Fig. S1). These boundary conditions (BCs) make our simulation equivalent to the indentation of a 200×100 mm film. No boundary conditions were applied to the indented edge and its opposite side. All our simulations were made using an elastic material definition with Young's modulus $E = 4.4$ GPa and Poisson ratio $\nu = 0.4$ since we found these values tabulated for Mylar films [S1]. However, these specific values do not restrict the generality of our conclusions because Young's modulus only scales the force, and Poisson ratio plays a small role in the von Kármán number.

The contact properties of the interactions between the indenter and the film are frictionless in the tangential direction and hard contact in the normal direction. We used the general contact algorithm to account for the contact between the film and cylinder and self contact interactions.

A typical numerical analysis was made first by using the explicit solver and exploring the indentation of the film for large displacement. Figure S2 shows the force displacement relation obtained using the explicit algorithm (gray line). Although the force displacement curve obtained is noisy (because of dynamic effects) and there is large numerical error produced at the first buckling instability, this solver captures subsequent buckling instabilities and wrinkling formation.

In a second stage, we used a dynamic implicit solver in its quasi-static application (red line in Fig. S2). We used imperfections to force the appearance of the first buckling instability and move the indenter to a safe displacement where the dynamic and explicit solver show similar results. This matching is obtained for $d = 1$ mm in Fig. S2. At that point we worked backwards by using the static solver to obtain good resolution and capture the compressive in-plane deformation before buckling (black line in Fig. S2).

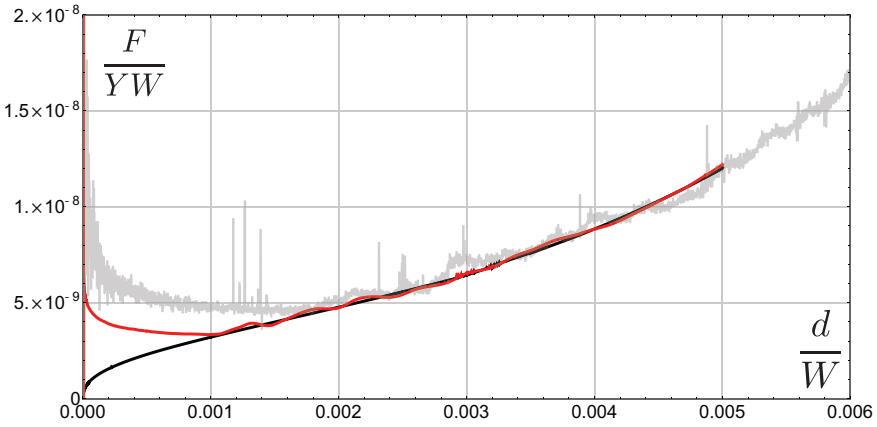

Fig. S 2. Force displacement response for $t = 0.5$ μm and the same parameters of Fig. 2 in the main text by using the dynamic explicit (gray line), dynamic implicit (red line) and static (black line) solvers. While the explicit and implicit algorithms are applied moving forward, the static algorithm is applied moving backwards. Dynamic effects at the buckling instability explain the large errors observed in the force displacement relation when using dynamic algorithms.

The numerical simulation was validated by comparing the force-displacement relation for large indentation with experimental data. Experimental and numerical data for large displacement must follow the pure stretching relation

$$F/(YW) = \Pi(d/W) \tag{S 1}$$

if they are elastic and the right Young's modulus is used to scale the force. Here $\Pi(x) =$

$\eta(16/3)x^4$ is a dimensionless function obtained from the theoretical analysis explained in the main text. To obtain parameter η, we fit the function $\Pi(x)$ to the numerical data for $t = 0.5$ μm shown in Fig. 2b and Fig. S3. The numerical data of Fig. S3 shows that the stretching dominated regime for this value of thickness becomes relevant for $x \gtrsim 10^{-2}$; hence, an appropriate region of displacement to fit the numerical data to the function $\Pi(x)$ is $x > 0.5$. The fit gives $\eta = 0.449$ that we approximate to $\eta \approx 0.5$ in the following.

To validate the numerical simulations, we use the experimental data for the OS film (the thinest of our materials) to obtain its Young's modulus by using a fit to the function $\Pi(x)$ with $\eta = 0.5$. The fit for large displacement provides the value $E = 5.7$ GPa, which is higher than the typical tabulated stiffness for Mylar films found in the literature [S1]. A traction experiment done for the same material using an Instron testing system with special tensile grips gives the value $E = 5.3$ GPa, which is consistent with the indentation experiment. Figure S3 shows the agreement between the numerical curve and the experimental data for large displacement when using the value $E = 5.7$ GPa as stiffness for the OS film. The experimental data is above the numerical data for small displacement due to dynamic effects that are characteristic near buckling conditions (see Fig. S2) and fluctuations that become important when using extremely thin materials.

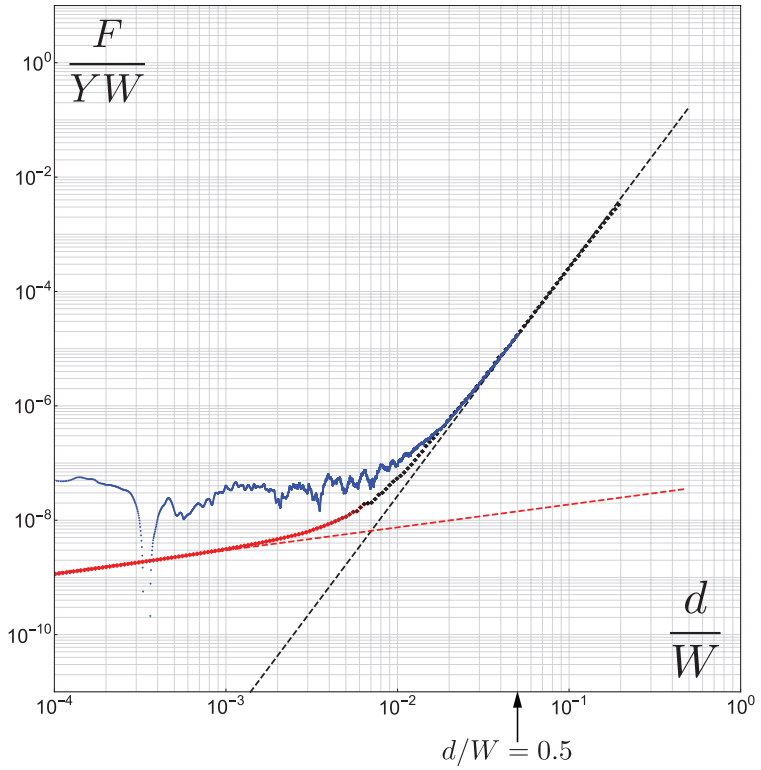

Fig. S 3. Experimental data (red dots) for OS film ($W = 200$ mm, $R = 0.5$ mm) in dimensionless form by using the Young's Modulus $E = 5.7$ GPa obtained from the best fit to the asymptotic curve $\Pi(x) = (8/3)x^4$ (black dashed line).

III. Sensitivity to Other Parameters

In the main text, we assume the general force-displacement relation

$$F/(YW) = \Pi(d/W, N) \tag{S 2}$$

that neglects the effect of the indenter radius R and the distance from the edge to the clamped boundaries H (see Fig. S4(a)).

To evaluate the importance of distance H, we numerically studied a simple extension of our main configuration by moving the clamped boundary to distance H and used symmetry BCs at that edge (YSYMM option). This is equivalent to indent the free edge in two opposite directions as shown in Fig. S4(b). Figure S5 shows the force displacement response for a film of thickness $t = 100$ μm for $H = 100$ mm (open triangles). Comparing with the case in which $H = 0$ (open circles), we observed differences at buckling conditions but the response is similar in the near threshold (NT) and far from threshold regime (FT). Moreover, the case with $H = 100$ mm approaches faster to the asymptotic limits in the NT and FT regimes. We expect a weak dependence on the parameter H based on the assumptions used in the main text to describe the force displacement response, in which strains are computed by the deformation of the free edge only.

We also studied the effect of the indenter radius in the force displacement response. The results of Fig. 2 in the main text are made with $R = 4$ mm and Fig. S5 includes the case in which an indenter of radius $R = 1$ mm is used (cross points). The differences between this case and the equivalent case for $R = 4$ mm (open circles) are small.

Free edge BCs at $y = L$ (see Fig. S1) were used in all the simulations shown in Fig. 2. To study the importance of the boundary conditions at the opposite side of the indented edge, we compare in Fig. S5 the results between using free edge (open circles) and clamped BCs (black circles) while the rest of the parameters are kept the same. The difference between these two simulations are indistinguishable.

A different response is observed when including friction in the system. We have used free-sliding conditions in all our simulations of Fig. 2 (main text) and the opposite case corresponds to using rough boundary conditions (no sliding) and adhesive contact. This means the film cannot move in the tangential direction, and after contact the film and the indenter are stuck. We physically expect this condition if the indenter is coated with a strong adhesive before indentation. The force, for equivalent displacement for the frictionless case,

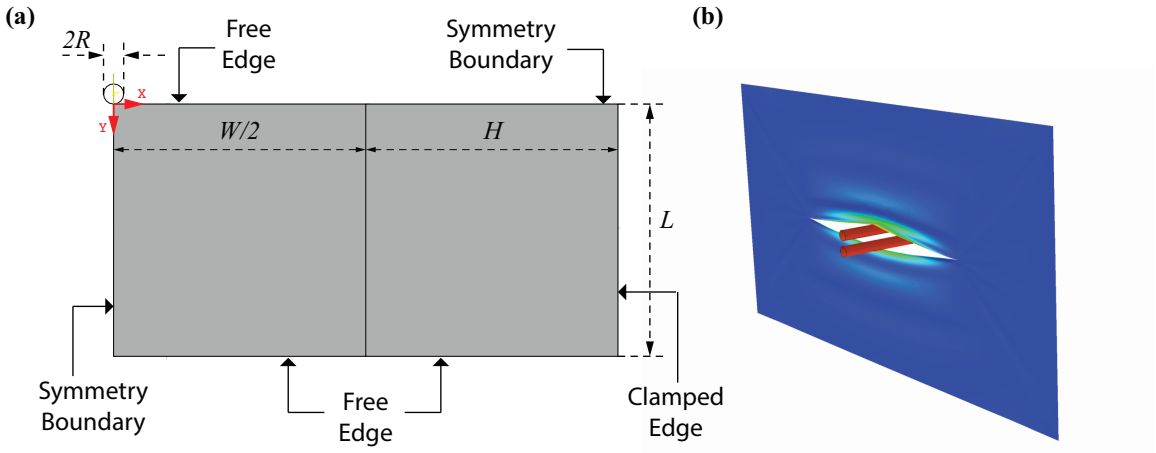

Fig. S 4. (a) Schematic of the setup to study the influence of the distance H from the ends of the cut to the clamped boundaries. The simulation and BCs defined in the figure correspond to the problem where two indenters are applied to the cut moving in opposite directions. (b) Deformation observed after mirroring the results obtained from Abaqus.

is much larger; however, this only changes the prefactor in the NT regime. The FT regime remains the same.

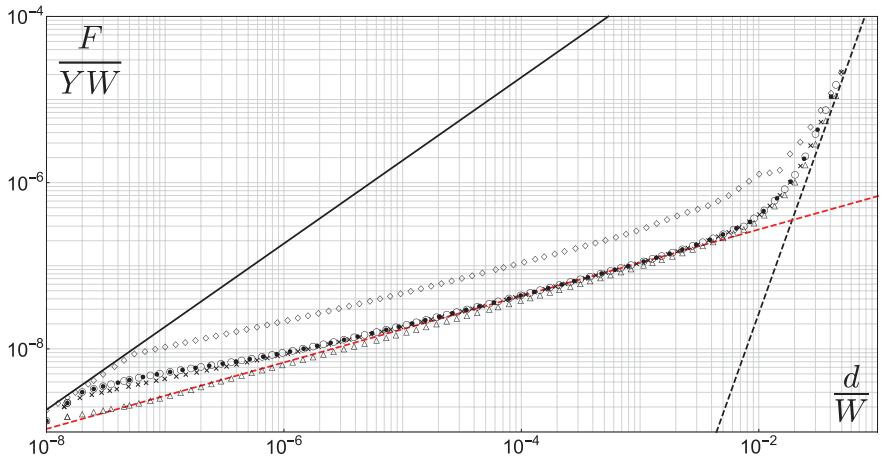

Fig. S 5. Force versus displacement for thickness $t = 100$ μm and different geometrical parameters. We used $[R, H]$=[4, 0] (millimeters, $\circ$) for the configuration defined in Section 1 and Fig. S1. We did for the same parameters two variations of the same configuration: i) a simulation with clamped BCs at the opposite side of the indented edge ($\bullet$), and ii) a simulation in which contact is completely rough and adhesive ($\diamond$). The simulation for $[R, H]$=[1, 0] (millimeters, $\times$) shows the effect of changing the indenter radius. The simulation for $[R, H]$=[4, 100] (millimeters, $\triangle$) corresponds to the geometry and BCs defined in Fig. S4. For all the simulations the width of the free edge is $W = 200$ mm, the length of the film is $L = 100$ mm, and the material parameters are $E = 4.4$ GPa, and $\nu = 0.4$. Solid and dashed lines are the same as shown in Fig. 2 in the main text.

IV. Buckling Analysis

The response before buckling is purely compressive and described by a linear relation between force and displacement. This relation is shown in Fig. S6(a) (solid black line) and follows the fit

$$F/(YW) = c_1(d/W) \tag{S 3}$$

where $c_1 \approx 0.19$. The prefactor is sensitive to the distance to the clamped boundaries H, the length of the film L (see Fig. S4), the BCs applied at the opposite side of the free edge, etc.. This is a typical Hertz contact problem [S3] that is well known so that we focus on the results for the specific BCs used in our simulations. It is noteworthy that the in-plane response of the material is affected by the BCs and geometrical configuration far from the free edge, but the NT and FT response are not.

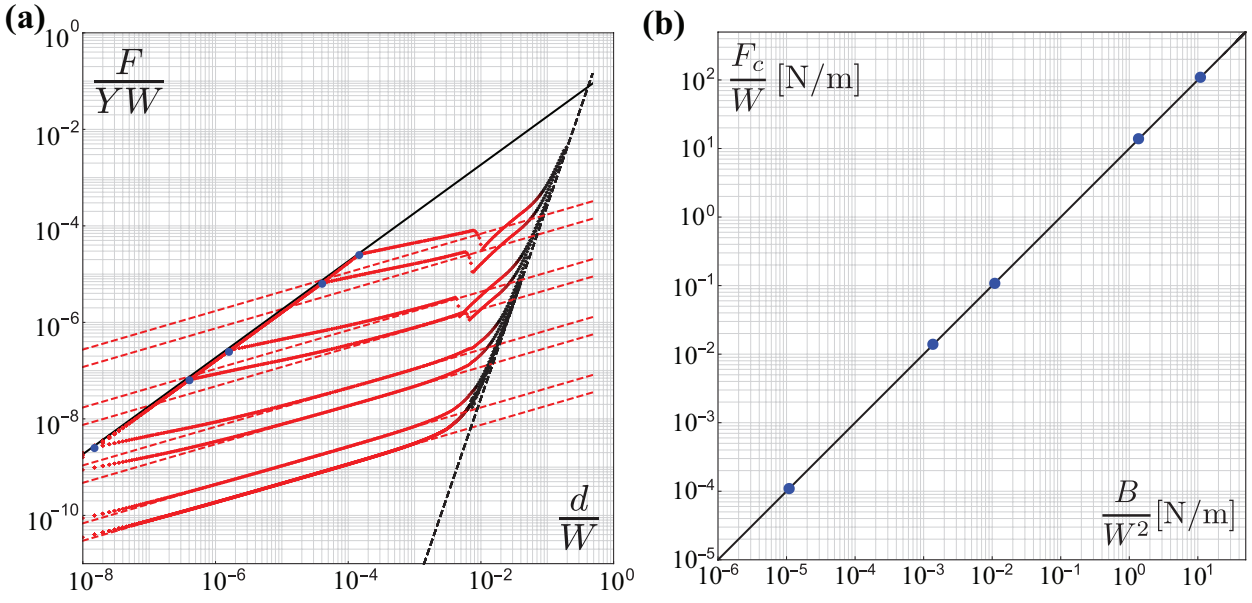

Fig. S 6. (a) Figure 2 of the main text with the critical force and displacement marked with blue dots for the thickness $t = 10, 50, 100, 500, 1000$ μm. Greater thickness requires greater critical force. (b) The critical force per unit of length, F_c/W, extracted from (a) are plotted as a function of the corresponding bending stiffness in the dimensional form B/W^2. Solid black line corresponds to Eq. S 4.

Using the numerical results we can extract the critical value for the force at the position of buckling. Figure S6(b) shows that the critical force per unit of width follows a linear

relation with the parameter B/W^2 which is

$$F_c/W = c_2 B/W^2 \tag{S 4}$$

where $c_2 \approx 10$ is obtained from a fit. The critical buckling force is expected based on exact calculations for more simple geometries found in textbooks. For example, the critical force for buckling of a compressed plate under constant force per unit of line F/W at $y = 0, L$ and clamped at $x = \pm W/2$ in which $L/W = 0.5$ (the case of Fig. S6) is given by $F_c/W = k\pi^2 B/W^2$ where $k \approx 7.69$ [S2]. We expect this force to be larger than the one given by Eq. (S 4) because a concentrated force must decrease the buckling threshold.

Using Eqs. (S 3) and (S 4), we conclude that the critical displacement at the position of buckling d_c/W is given by

$$\frac{d_c}{W} = c_3 \frac{B}{YW^2} = c_3 N^{-2} \tag{S 5}$$

where $c_3 \approx c_2/c_1 = 52.6$.

V. Tension Analysis

To study the tension T along the x direction, we used the total sectional force along the centerline of the film, $\tau = \int_0^\infty dy \vec{f}(\hat{x}) \cdot \hat{x} = \int_0^\infty dy \sigma_{xx}$. Based on the assumptions made for the tension, we obtained for the total sectional force the scaling $\tau/(YW) \approx T\lambda/(YW) \approx N^{-4/5}(d/W)^{3/5}$ in the NT regime, while $\tau/(YW) \approx Td/(YW) \approx (d/W)^3$ in the FT regime.

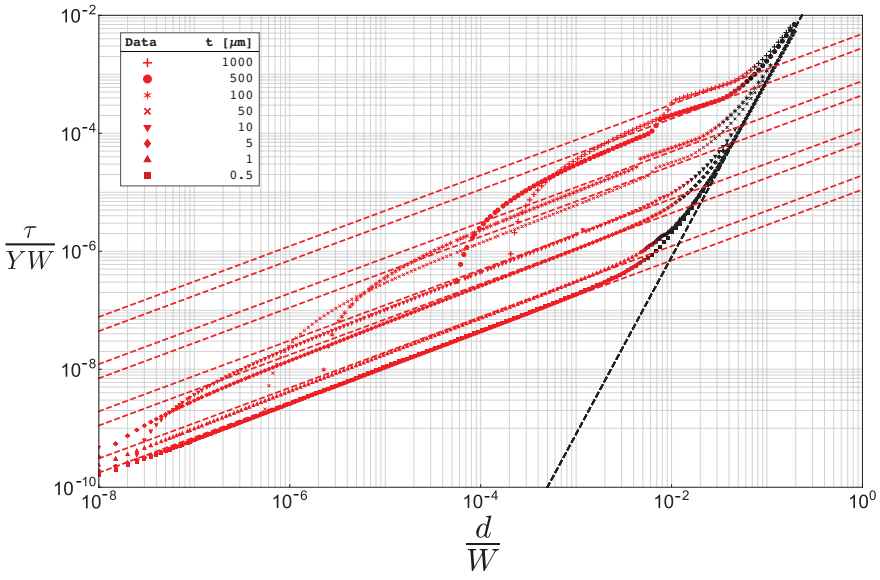

Fig. S 7. Total cross-sectional force versus displacement. The simulations are for the same parameters of Fig. 2 in the main text. The red dashed lines correspond to the scaling of Eq. (S 6) for the NT regime so that their positions change with the von Kármán number, or equivalently, the thickness of the film. In contrast, the black dashed line represents the FT regime given in Eq. (S 7) and corresponds to a pure stretching limit. Here we used the same color map as shown in Fig. 2 of the main text.

Figure S7 confirms these scalings. Specifically, we obtained for the NT regime the fit

$$\frac{\tau}{YW} = c_4 \left(\frac{d^3}{W^3 N^4} \right)^{1/5} \tag{S 6}$$

and for the FT regime

$$\frac{\tau}{YW} = c_5 \left(\frac{d}{W}\right)^3 \tag{S 7}$$

Here $c_4 \approx 0.85$ and $c_5 \approx 0.8$.

[S1] Cammarano, A., De Luca, G. & Amendola, E. Surface modification and adhesion improvement of polyester films. *Cent. Eur. J. Chem* **11**, 35-45 (2013).

[S2] Timoshenko, S.P. & Gere, J.M. *Theory of Elastic Elasticity* (McGraw-Hill, New York, 1988).

[S3] Barber, J.R. *Elasticity* (Springer, New York, 2010).